RSC Advances

PAPER

View Article Online
View Journal | View Issue



Cite this: *RSC Adv.*, 2017, **7**, 10278

# Efficient production of acrylic acid by dehydration of lactic acid over $BaSO_4$ with crystal defects†

Shuting Lyu and Tiefeng Wang*

Received 20th December 2016
Accepted 31st January 2017

DOI: 10.1039/c6ra28429a

rsc.li/rsc-advances

$BaSO_4$ catalysts with different micromorphologies and crystal texture were prepared and used to investigate the structure–activity relationship in the dehydration reaction of lactic acid (LA) to acrylic acid (AA). SEM and $N_2$ physisorption were used to study the micromorphology. XRD and photoluminescence spectra were employed to analyze the crystal texture of samples prepared with different methods and treatments. The results revealed that $BaSO_4$ with smaller crystals and more defects had higher activity and selectivity to AA. It was likely that the crystal defects provided the active acid sites for dehydration of LA to AA, as evidenced by XPS and $NH_3$-TPD measurements. Using ethanol as the solvent and ultrasound treatment during the preparation of $BaSO_4$, imperfect small crystals with more defects were formed, which increased the AA selectivity to 78.8%.

## 1. Introduction

Lactic acid (LA), one of the most important biomass derived platform chemicals, is regarded as a promising alternative resource due to the excessive depletion of fossil resources.[1,2] With two functional groups, LA has wide applications in the food industry, commodity chemicals and biopolymers.[3,4] LA can be produced by traditional microbial fermentation[5] or glycerol dehydrogenation.[6] In a recent work, LA was produced with a high yield of 70% by catalytic conversion of biomass raw materials such as lignocellulose.[7]

LA can be converted into valuable chemicals by a variety of catalytic processes, among which the dehydration of lactic acid to acrylic acid (AA) attracts particular attention,[8] because AA is widely used in the manufacture of paint additives, adhesives, textiles, leather treating agents and synthetic resins. Currently, the industrial production of AA mainly depends on petroleum-based propylene or propane as feedstocks, which is costly and unsustainable.[6] Therefore, the development of a sustainable process for conversion of LA to AA is of great significance.

The main side products in dehydration of LA are acetaldehyde (AD) and $CO_x$ from decarbonylation and decarboxylation, propionic acid (PA) from hydrogenation, and 2,3-pentanedione from condensation. Non-catalytic self-esterification and polymerization can also produce some side products.[9] Further side products such as acetic acid (AcOH) are produced from oxidization of acetaldehyde or carbonylation of propionic acid.[10] Diverse reaction pathways of LA with or without catalysis make it challenging to increase the yield of AA in dehydration of LA.

The early research on dehydration of LA focused on mixed metal phosphates and sulfates as catalysts. In 1958, mixed sulfates of $Na_2SO_4/CaSO_4$ with molar ratio of 1 : 25 was reported to give an AA yield of 68% at 400 °C.[11] However, little attention was attracted at that time and the mechanisms of LA reaction such as dehydration and decarbonylation/decarbonylation were not studied until the last decade. Studies on different zeolites modified with alkali/alkali-earth metal salts revealed that weak and medium acid sites were active sites in the dehydration reaction,[12–14] while some reported that a kind of cooperative acid–base catalysis also help during the dehydration of LA to AA.[12,15,16] Decarbonylation and decarboxylation, known as the most important side reactions, were mainly catalyzed by strong acid sites and were enhanced under high reaction temperature.[13,17] The surface hydroxyl groups could also lead to particular adsorption mode favoring decarbonylation/decarbonylation to AD, evidenced by later study on the alkaline earth hydroxyapatites.[18] In the early period, extensive studies were conducted on different zeolites modified with alkali/alkali-earth metal salts to improve the catalysis efficiency.[12,13,17,19–23] However, the durability of the alkali/alkali-earth modified zeolites is a big problem because of the deactivation, instability of framework and loss of surface modifiers under the atmosphere of water vapor and high temperature.[24] Recently, more attentions were paid to phosphates and sulfates of alkaline earth metal.[18,25–28] Vidhya *et al.* reported a 60% selectivity over calcium hydroxyapatite (HAP) catalysts, and proposed the possible mechanism of LA conversion to AA and AD.[25] Barium sulfate and the $Ca_3(PO_4)_2$–$Ca_2P_2O_7$ (50 : 50 wt%) catalysts were reported to give high AA selectivity of 74% and 76%, respectively.[28,29] However, the

*Beijing Key Laboratory of Green Reaction Engineering and Technology, Department of Chemical Engineering, Tsinghua University, Beijing 100084, China. E-mail: wangtf@tsinghua.edu.cn*

† Electronic supplementary information (ESI) available. See DOI: 10.1039/c6ra28429a

knowledge of the relationship between acidity of sulfate catalysts and the selectivity to acrylic acid is still limited.

In the present work, we studied the $BaSO_4$ catalysts to identify the reactive sites in sulfate for dehydration of LA to AA. Different preparation methods were used to change the textures and acidities of the $BaSO_4$ catalysts. The catalytic performance was correlated with the surface and microscopic characteristics, suggesting that crystal defects provided the required weak and medium acid sites, which were the essential active sites for LA conversion and AA formation. A high selectivity to AA was achieved over the optimized active $BaSO_4$ catalyst.

# 2. Experimental

## 2.1. Catalyst preparation

The $BaSO_4$ catalysts were purchased or prepared by co-precipitation using $(NH_4)_2SO_4$ and $BaCl_2 \cdot 2H_2O$ as precursors. Firstly, 0.03 mol $(NH_4)_2SO_4$ and 0.03 mol $BaCl_2 \cdot 2H_2O$ were separately dissolved in 120 mL distilled water. The obtained $BaCl_2$ solution was added to the $(NH_4)_2SO_4$ solution dropwise to form white precipitate of barium sulfate, which was washed, dried at 80 °C in air overnight, and then calcined at 500 °C for 4 h to obtain the catalysts denoted as Co-pre. Other $BaSO_4$ samples with different crystal defects were prepared using different solvents (water and ethanol) and ultrasonic treatment in the precipitation process. In a typical experiment, the obtained $(NH_4)_2SO_4$ solution and $BaCl_2$ solution were added to the solvent (*e.g.* ethanol) co-currently to form white precipitate of barium sulfate, which was treated with ultrasound immediately for 15 min. Aging for varied time, the white precipitate was also washed, dried at 80 °C in air overnight, and then calcined at 350, 500, 600 and 700 °C for 4 h to obtain the catalysts denoted as EtOH/ult-*m*h-*T*, in which EtOH represented the solvent ethanol, *m* was the aging time in hour, and *T* was the calcination temperature in Celsius.

## 2.2. Catalyst characterization

The morphology of the catalysts were characterized with the field emission scanning electron microscopy (SEM, JSM 7401F, JEOL, Japan). The BET surface area and pore volume were calculated from nitrogen adsorption–desorption isotherms measured at 77 K on a physical adsorption apparatus (Quandasorb-SI-4, Quantachrome) after degassing the sample at 573 K. The composition and texture of the catalysts were identified by an X-ray powder diffractometer (XRD, Bruker-AXS D8 Advance, Germany), using Cu K$\alpha$ ($\lambda$ = 0.154178 nm) radiation. The scanning of enlarged (121) diffraction peaks was specially conducted at a rate of 0.1° $min^{-1}$ to provide precise information for calculation of the interplanar spacing and crystal size. The contents of crystal defects were characterized by the room temperature photoluminescence spectra (PL). The measurement was conducted on a Hitachi F-7000 luminescence spectrometer, using a Xe lamp with an excitation wavelength of 325 nm. The surface composition and chemical states of the samples were characterized by an X-ray photoelectron spectrometer (XPS, Thermal Scientific ESCALAB 250Xi). $NH_3$-TPD was carried out to determine the acidity of catalysts using an automated adsorption system (ChemBET Pulsar TPR/TPD, Quantachrome) with a thermal conductivity detector (TCD). For each $NH_3$-TPD experiment, a sample of 600 mg was placed in a quartz tubular reactor and pretreated at 350 °C with a He flow of 30 mL $min^{-1}$ for 30 min, simulating the sample pretreatment in the catalytic reactor prior to the reaction. The sample was cooled to 80 °C, and then 5% $NH_3$/He was introduced at a flow rate of 30 mL $min^{-1}$ for 30 min at 80 °C, and then the sample was purged in He stream until a constant TCD level was obtained. The reactor temperature was programmed at a rate of 10 °C $min^{-1}$ to 600 °C and the desorbed $NH_3$ was detected online by the TCD. Considering the pretreatment temperature, the signals above 350 °C could be assigned to the evolution of $NH_3$ from the thermal decomposition of ammonium or carbonate residues in the samples, and had no effects on the overall acidity of the samples.[15]

## 2.3. Catalytic reaction

The catalysts were evaluated for the dehydration of LA in a fixed-bed quartz reactor (11 mm i.d.) using 0.25–1 g of catalyst at 350 °C under atmospheric pressure. An aqueous solution of 20 wt% LA (1.2 mL $h^{-1}$) was fed into the reactor by a HPLC pump (Series 3, 0.01–5 mL $min^{-1}$, SS, S. G. Seal Self Flush, Pulse Damper) with nitrogen (30 mL $min^{-1}$) as carrier. The contact time, decided by all these reaction conditions, were calculated according to the literature.[30] All the reactants and products were preheated to 160 °C to avoid undesired condensation.[26] The reaction products and unconverted LA were collected in a cold trap of −5 °C and analyzed offline by gas chromatograph (GC 7900, Techcomp Ltd.) equipped with a FID detector and a TM-SuperWax column (30 m × 0.25 mm × 0.25 μm, Techcomp Ltd.). The reaction was conducted for 9 h, and the products of the first three hours were not taken into account because they did not satisfy a good mass balance. A comprehensive evaluation result for the sample was derived by solving the average conversions or selectivities during 4–9 h. The LA conversion and product selectivity were calculated by

$$\text{LA conversion} = 1 - \frac{\text{moles of unconverted LA}}{\text{moles of LA in the feed}} \times 100\%$$

$$\text{Product selectivity} = \frac{\text{moles of a defined product}}{\text{moles of converted LA}} \times 100\%$$

# 3. Results and discussion

## 3.1. Catalyst characterization

**3.1.1. Morphology and $N_2$ physisorption.** The morphology and microstructure of the $BaSO_4$ catalysts prepared with different methods differed significantly from each other, as shown in Fig. S1† and summarized in Table 1. The commercial $BaSO_4$ sample had large particle size of 0.2–1.2 μm and had no pore structure. The samples prepared in water with or without ultrasonic treatment were similar in particle size and pore

Table 1 Textural and acid properties of $BaSO_4$ prepared with different methods

| Catalyst | Particle size[a] (μm) | Surface area ($m^2$ $g^{-1}$) | Pore volume (mL $g^{-1}$) | Interplanar spacing[b] (nm) | Crystal size[b] (nm) | Acid amount (μmol $g^{-1}$) |
|---|---|---|---|---|---|---|
| Commercial | 0.2–1.2 | 4.2 | 0.006 | 0.3102 | — | 0.21 |
| Co-pre | 0.1–0.6 | 10.1 | 0.027 | 0.3104 | — | 4.08 |
| Water/ult | 0.1–0.8 | 9.5 | 0.024 | 0.3088 | — | 6.83 |
| EtOH/ult-0 h-500 | 0.03–0.3 | 20.0 | 0.102 | 0.3063 | 60.0 | 21.15 |
| EtOH/ult-1 h-500 | 0.03–0.3 | 18.5 | 0.095 | 0.3081 | 66.7 | 19.04 |
| EtOH/ult-2 h-500 | 0.03–0.3 | 17.9 | 0.094 | 0.3096 | 72.9 | 18.22 |
| EtOH/ult-24 h-500 | 0.03–0.3 | 17.7 | 0.093 | 0.3099 | 79.4 | 17.92 |
| EtOH/ult-0 h-350 | 0.03–0.3 | 17.4 | 0.069 | 0.3063 | 84.1 | 6.92 |
| EtOH/ult-0 h-600 | 0.03–0.4 | 15.8 | 0.073 | 0.3070 | 87.3 | 11.22 |
| EtOH/ult-0 h-700 | 0.1–0.8 | 5.9 | 0.031 | 0.3072 | — | 2.22 |

[a] Determined by SEM. [b] Determined by enlarged (121) diffraction peaks of XRD patterns.

structure, while the ultrasound treated sample exhibited smaller pores. In comparison, the catalysts prepared in ethanol with ultrasound, EtOH/ult, had a much smaller particle size, with most particles under 300 nm. The smaller pores of EtOH/ult samples were also detected by TEM (Fig. S1e†) and confirmed by $N_2$ physisorption in Table 1.

The specific surface area and pore volume for all the $BaSO_4$ catalysts are summarized in Table 1. The first four rows exhibited considerable differences in surface area (4.2 to 20.0 $m^2$ $g^{-1}$) and pore volume (0.006 to 0.102 mL $g^{-1}$) among the samples prepared with different methods. The BET surface area and pore volume of the commercial sample were very low due to its big particle size and nonporous structure. The samples synthesized in water with and without ultrasonic treatment exhibited similar medium surface area and pore volume. In contrast, the catalysts prepared in ethanol had much higher surface area and pore volume because they had smaller particle size and porous structure. These results indicated that the solvent had more significant effects on the particle morphology than ultrasound treatment. Because of the lower solubility of precursors, ethanol could reduce the particle size and restrain the particle growth.[31–33]

Entries 4 to 10 compared the EtOH/ult samples with different aging time or different calcination temperature (350 to 700 °C). When the aging time increased from 0 to 24 h, the BET surface area slightly decreased from 20.0 to 17.7 $m^2$ $g^{-1}$, and the pore volume decreased from 0.102 to 0.093 mL $g^{-1}$, indicating slow crystal growth during the aging process. Entries 8 to 10 showed that the increase of calcination temperature led to a sharp decline of surface area, especially at 700 °C, which could be attributed to the accelerated recrystallization under high temperatures. The recrystallization increased the particle size and decreased the surface area. An exception was the sample calcined at 350 °C, which displayed a lower surface area than that at 500 °C due to the undesired carbonization of adsorbed ethanol on the catalyst surface, as confirmed by its ash appearance and the TG measurement (Fig. S2†).

**3.1.2. XRD patterns.** Fig. 1 shows the XRD patterns of the samples prepared with different methods. All the peaks of the four catalysts can be indexed to the $BaSO_4$ (JCPDS 24-1035). However, compared with the standard (121) position, Fig. 1(b) indicated the right shift of the (121) peaks for the catalysts prepared with ultrasonic treatment both in water and ethanol solvents. The left and right shifts of the diffraction peaks were attributed to the defect-induced lattice expansion and contraction respectively, according to previous studies.[34–36] The interplanar spacing was calculated from Bragg equation, and the results are listed in Table 1. According to the theory of crystal, the generation of defects is usually stimulated by heteroatom or energy. Therefore, ultrasonic treatment could facilitate the generation of defects, evidenced by the reduced interplanar

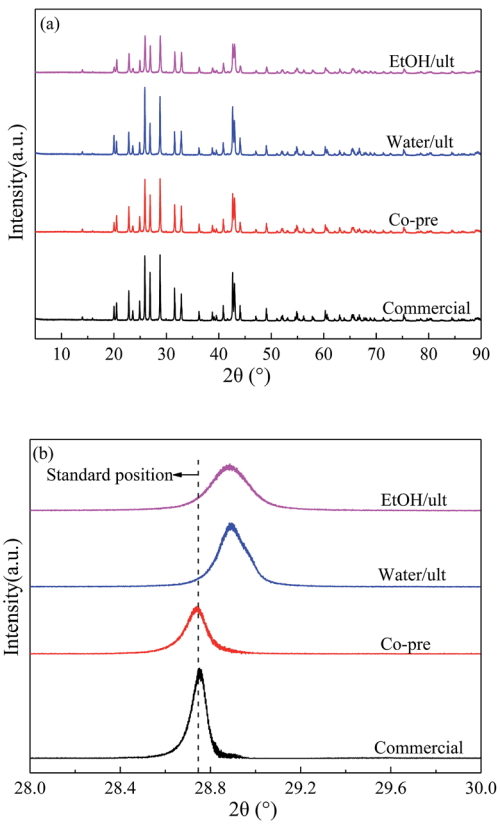


Fig. 1 (a) XRD patterns and (b) enlarged (121) diffraction peaks of $BaSO_4$ catalysts prepared with different methods.

spacing of Water/ult and EtOH/ult catalysts. The crystal size was calculated from Scherrer's formula, and the results are listed in Table 1. Only the EtOH/ult samples have crystal size smaller than 100 nm, while those purchased or prepared with other methods were beyond the application range of Scherrer's formula. These small crystals had poor integrality and provided more crystal defects.

The enlarged XRD (121) diffraction peaks of $BaSO_4$ aged for different time were compared in Fig. 2(a). With the increase of aging time, the shift of the (121) diffraction peak gradually decreased, indicating that the interplanar spacing became closer to the standard value (entries 4–7 in Table 1) and the integrality of crystals was improved. Meanwhile, the full width at half maximum (FWHM) of the (121) diffraction peak decreased from 0.169° to 0.158°, 0.151° and 0.144° when the aging time increased from 0 to 1, 2 and 24 h respectively, indicating that the crystal grew larger with longer aging time (Table 1). These results revealed that the defect-induced lattice contraction was gradually eliminated due to the improvement of crystal integrality and the reduction of defects during the aging process. The $BaSO_4$ sample prepared without aging had the most significant crystal defects among these four samples.

Fig. 2(b) compared the crystal textures of the $BaSO_4$ samples calcined at different temperatures. The left shift of diffraction peak only slightly reduced with increasing calcination temperature, suggesting that the calcination temperature had insignificant effect on the crystal defects. In addition, the crystal size displayed a modest growth with the calcination temperature increasing from 500 °C to 700 °C (Entries 4, 9 and 10 in Table 1). The abnormally larger crystal size observed in the sample calcined at 350 °C was likely attributed to the residue of deposited ethanol in crystals. Combined with the discussion on the particle size and morphology in 3.1.1, it can be concluded that the high-temperature calcination significantly increased the particle size and reduced the pore structure, but only slightly affected the crystal textures and defects.

**3.1.3. Photoluminescence spectra.** Photoluminescence (PL) analysis was used to characterize the optical properties of the $BaSO_4$ samples, which were related to the defect states. The relative PL intensities were employed to compare the contents of crystal defects in samples characterized under the same conditions.[35] Here all the samples were analyzed and EtOH/ult catalysts with different aging time were discussed as a typical series for its characteristic variation in crystal defects. As shown in Fig. 3, all the samples exhibited a broad peak in the region of 350–650 nm, including the ultraviolet emissions at around 390 nm and the green emissions centered at 517 nm. With the increase of aging time, the PL intensities of both the ultraviolet and green emission decreased, indicating a decrease of the amount of defects in the $BaSO_4$ samples.[35] Consistent with the XRD patterns discussed in 3.1.2, the PL spectra in Fig. 3 confirmed that the amount of crystal defects in $BaSO_4$ samples was enhanced with ultrasonic treatment in ethanol solvent, and the aging process significantly reduced the amount of crystal defects. Difference in the amount of crystal defects were also found with the $BaSO_4$ prepared by different methods (Fig. S3a†) and EtOH/ult catalysts calcined at different temperature (Fig. S3b†).

**3.1.4. X-ray photoelectron spectrometer.** The S2p and O1s binding energies (BEs) of the $BaSO_4$ samples with different aging time were analyzed by XPS, and the results were listed in Table 2. The S2p and O1s BEs increased with increasing aging

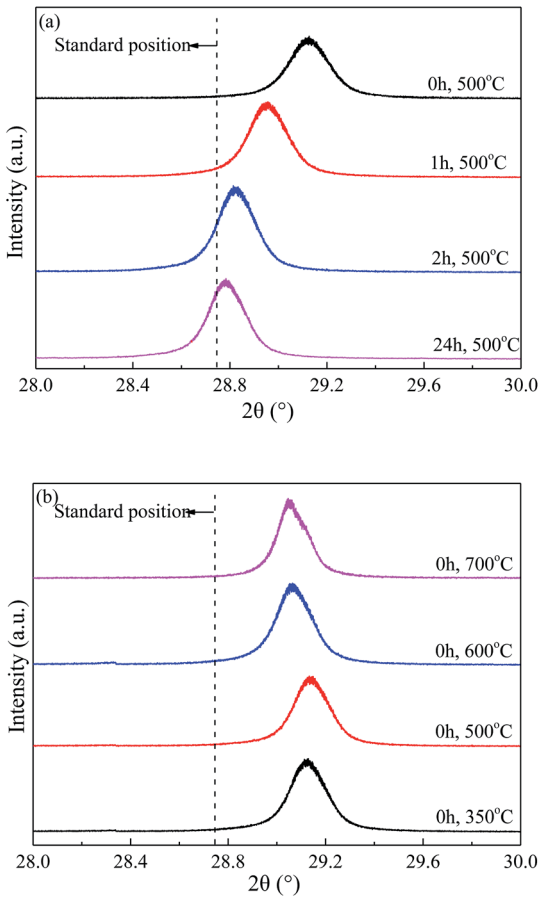


Fig. 2 Enlarged XRD (121) diffraction peaks of $BaSO_4$ catalysts (a) aged with varied time length and (b) calcined at different temperature.

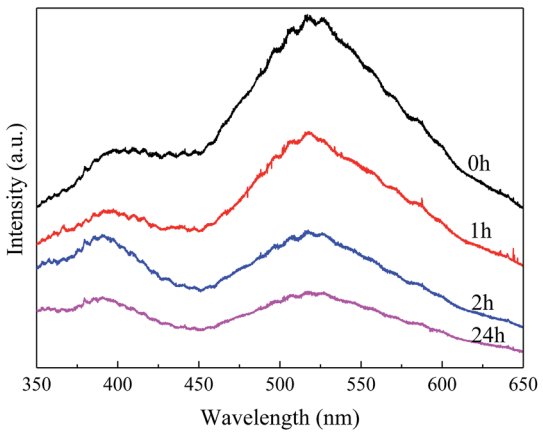


Fig. 3 Photoluminescence (PL) spectra of $BaSO_4$ catalysts with different aging time.

Table 2 S2p and O1s binding energies of $BaSO_4$ aged with varied time

| Aging time (h) | 0 | 1.0 | 2.0 | 24.0 |
|---|---|---|---|---|
| S2p BE, eV | 168.82 | 168.82 | 168.86 | 168.89 |
| O1s BE, eV | 531.85 | 531.90 | 531.96 | 531.98 |

time, indicating that aging process decreased the electron density of the sample, which could be attributed to the lower density of defects. According to the theory of point defects,[37–39] especially the Frankel defects, it is quite common in ionic crystal that cations escape from their normal sites, thus become interstitial atoms and produce vacancies. Vacancies and interstitial atoms always form in pairs, and provide sites with unbalanced electrons. The escaped cations are electropositive and act as Lewis acid, and the electronegative vacancies can donate electrons and act as basic sites. In the EtOH/ult samples, these vacancies caused by defects partly disappeared after aging, leading to a decrease in the electron density and an increase in BEs. The EtOH/ult-0 h catalyst had the largest amount of basic sites, which favored the generation of AA.[12,15]

**3.1.5. Acid properties.** The temperature programmed desorption (TPD) of $NH_3$ was carried out to evaluate the amount and strength of acid sites of the different $BaSO_4$ catalysts (Fig. 4 and S4†). The acid amount was calculated by integrating the TPD peaks, and the results were listed in Table 1. The $BaSO_4$ catalysts showed weak and medium acidity with a broad desorption peak from 150 to 350 °C, except that the commercial $BaSO_4$ had no adsorption of $NH_3$.

As shown in Table 1 and Fig. 4, the EtOH/ult $BaSO_4$ sample had the highest acid amount of 21.15 μmol $g^{-1}$, indicating that ethanol solvent and ultrasound treatment enhanced the formation of surface acid sites. In contrast, the acid amount of Water/ult sample was only 6.83 μmol $g^{-1}$, mainly because the change of solvent significantly affected the particle size and surface area. Nevertheless, both the EtOH/ult and Water/ult samples had larger acid amount than the Co-pre sample, which confirmed the positive effect of ultrasonic treatment.

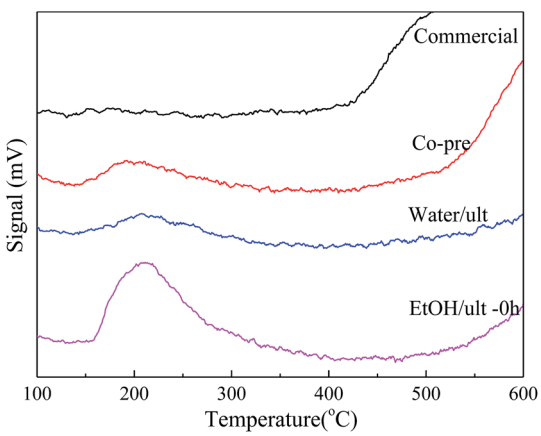


Fig. 4 $NH_3$-TPD profiles of $BaSO_4$ catalysts prepared with different methods.

Meanwhile, the peak temperatures of desorption were 192, 207 and 211 °C for the Co-pre, Water/ult and EtOH/ult samples, respectively, indicating that the catalyst acidity became slightly stronger when using ethanol solvent and ultrasonic treatment.

The $NH_3$-TPD results of the EtOH/ult samples with varied aging time were compared in Fig. S4(a).† With increasing aging time, the overall acid amount slightly decreased, as listed in Table 1. The decrease of acidity amount was attributed to the decrease of defects, especially the point defects, which was revealed by the XPS and shift of XRD diffraction peaks. These defects accompanied with local imbalance of electrons can provide the active adsorption sites for $NH_3$. With the increase of aging time, the amount of defects decreased and resulted in the reduction of acid sites.

The $NH_3$-TPD profiles of the $BaSO_4$ samples calcined at different temperatures are shown in Fig. S4(b).† The calcination temperature had significant effects on the acidic properties. The catalyst calcined at 350 °C was not considered because of the undesired carbonization of the deposited ethanol on the surface. The peak temperature of desorption decreased from 211 to 195 °C when the calcination temperature increased from 500 to 700 °C. In addition, the acid amount significantly decreased with increasing calcination temperature, and the largest acid amount was obtained with the catalyst calcined at 500 °C. One reason was the notable decrease of surface area which directly reduced the acid amounts, because $NH_3$ molecules and reactants were only adsorbed on the surface. However, this was not the only reason. Note that the acid density also decreased, some acid sites should also disappeared under high temperature, consisting with the unstable feature of crystal defects with a higher electron density. This result further confirmed that these crystal defects acted as acid sites and they were unstable under high temperatures.

### 3.2. Catalytic evaluation

**3.2.1. Effect of catalyst preparation method.** The dehydration reaction of lactic acid was conducted to compare the catalytic performance of the $BaSO_4$ samples prepared with different methods. The reaction conditions and results were summarized in Table 3, in which some typical catalysts in the literature were also included for a better comparison. The EtOH/ult-0 h-500 catalyst was evaluated for the dehydration of LA to AA from 300 °C to 400 °C. As shown in Table S2,† the best catalyst performance was obtained at 350 °C, which was used when evaluating other catalysts and comparing with the results in the literature. The conversion of lactic acid and selectivity to acrylic acid were plotted as a function of the time on stream, as shown in Fig. S5.† An induction period existed in the first 3 h, during which a considerable change of selectivity was observed for all the four catalysts. For better comparison, the average selectivity and conversion were calculated using the data during 4–9 h of reaction.

The commercial $BaSO_4$ catalyst showed a low LA conversion of 29.8% and a low AA selectivity of 28.8%. In contrast, the other three catalysts prepared in this work had enhanced LA conversion and AA selectivity. The Co-pre and Water/ult catalysts

 

Table 3 Catalytic performances of $BaSO_4$ prepared with different methods in this work and typical catalysts in the literature

| Catalyst | Reaction conditions | | | | Conversion (%) | Selectivity (%) | | Ref. |
|---|---|---|---|---|---|---|---|---|
| | $T$ (°C) | $N_2$ flow (mL $min^{-1}$) | Space velocity ($h^{-1}$) | Contact time (s) | | AA | AD | |
| Commercial | 350 | 30 | 2.5 (WHSV) | 0.19 | 29.8 | 28.8 | 41.2 | This work |
| Co-pre | 350 | 30 | 2.5 (WHSV) | 0.19 | 69.5 | 65.8 | 23.2 | |
| Water/ult | 350 | 30 | 2.5 (WHSV) | 0.19 | 70.1 | 69.7 | 18.0 | |
| EtOH/ult | 350 | 30 | 2.5 (WHSV) | 0.19 | 77.6 | 78.9 | 12.7 | |
| EtOH/ult | 350 | 30 | 5.0 (WHSV) | 0.10 | 66.1 | 76.7 | 16.4 | |
| $Na_2HPO_4$/NaY | 350 | 30 | 2.7 (LHSV) | 0.61 | 78.3 | 72.3 | 5.6 | 30 |
| $HAP_{1.62}$-360 | 360 | 15.5 | 1.4 (WHSV) | — | 84 | 74 | 18 | 21 |
| $BaSO_4$ | 400 | 1 | 2.1 (WHSV) | 0.5 | 100 | 74 | — | 28 |

showed similar LA conversion of 69.5% and 70.1%, respectively, while Water/ult had a slightly higher AA selectivity (69.7%) than Co-pre (65.8%). Among all the prepared catalysts, EtOH/ult had the best performance with 77.6% LA conversion and 78.9% AA selectivity under the same reaction condition. By decreasing the space velocity, the LA conversion increased to 97.5% while maintaining the selectivity to AA (Table S3†). As shown in Table S1,† the EtOH/ult catalyst had carbon balance close to 100%, indicating that the reaction data were reliable and the amount of other unknown side products was very low. However, some other catalysts had lower carbon balance, due to the poor selectivity to AA and formation of heavier products that could not be detected by GC. Considering the typical catalysts shown in Table 3, the $HAP_{1.62}$-360 catalyst was evaluated within TOS = 6–8 h,[21] and the $Na_2HPO_4$/NaY and $BaSO_4$ catalysts were evaluated within TOS = 2 h.[28,30] Overall, the EtOH/ult catalyst had a higher efficiency of AA production than the typical catalysts in the literature.[21,28,30] In the work of Peng *et al.*, the $BaSO_4$ catalyst was reported to have an AA selectivity of 74% and LA conversion of 100% at a contact time of 0.5 s and temperature of 400 °C. In this work, the EtOH/ult $BaSO_4$ catalyst had a LA conversion of 77.6% at a much shorter contact time (0.19 s) and much lower temperature (350 °C), suggesting EtOH/ult had a higher activity. In addition, EtOH/ult showed slightly higher selectivity to AA.

The difference in the catalyst activity could be attributed to the difference in acid amounts. With increasing crystal defects (Fig. S3a†) and surface area (Table 1), much more acid sites were observed with the EtOH/ult catalyst, which were the active sites of LA conversion.[12–14] In addition, the EtOH/ult catalyst showed a higher AA selectivity (78.9%) than the Co-pre (65.8%) and Water/ult catalyst (69.7%), due to their difference in weak and medium acid amount. In this work, the acid sites of all $BaSO_4$ catalysts were of weak to medium strength, which were suitable for the dehydration of LA to AA.[14,40] Few strong acid sites were observed, indicating that no undesired active sites were provided. Thus, most of the side reactions occurred without catalysis or on other sites such as the surface hydroxyl groups.[9,13,17,18] The increase of suitable acid sites enhanced the effective adsorption and subsequent dehydration of LA to AA, while the side reactions such as the decarbonylation/decarboxylation and polymerization were therefore maintained or suppressed by the promotion of the main dehydration reaction. As a result, both the LA conversion and AA selectivity were enhanced. Furthermore, the synchronous increase of acid sites and crystal defects indicated that the formation of acidity could be attributed to the escaped cations in crystal defects.

**3.2.2. Effect of catalyst aging time.** In order to compare the performance of the catalysts, a higher space velocity (WHSV = 5 $h^{-1}$) was used, considering that the catalyst activity could be better distinguished at a lower conversion. The aging time of EtOH/ult samples significantly affected the catalyst performance. As listed in Table 4, both the LA conversion and AA selectivity decreased with the increase of aging time. The EtOH/ult-24 h catalyst had the lowest LA conversion and AA selectivity, and EtOH/ult-0 h had the best catalytic performance (66.1% LA conversion and 76.7% AA selectivity). The LA conversion, AA selectivity, acid amount and crystal size were correlated for the EtOH/ult-*m*h samples in Fig. 5. It was found that the increase of crystal size distinctly decreased the acid amount, which in turn decreased both the LA conversion and AA selectivity. As illustrated in the analysis of XRD patterns, the growth of crystals improved the crystal integrality and reduced the crystal defects, which were also evidenced by XPS (Table 2) and PL measurement (Fig. 3). Thus, the increase of crystal size caused reduction of crystal defects. These results revealed that the decrease of crystal defects in the EtOH/ult catalysts decreased the amount of acid sites that were active for LA dehydration, thus decreased the LA conversion and AA selectivity. This relationship was consistent with the results of catalysts prepared with different methods.

Table 4 Effect of aging time on catalytic performance of EtOH/ult-500 catalysts[a]

| Catalyst | Conversion (%) | Selectivity (%) | | | |
|---|---|---|---|---|---|
| | | AA | AD | AcOH | PA |
| EtOH/ult-0 h-500 | 66.1 | 76.7 | 16.4 | 2.9 | 2.0 |
| EtOH/ult-1 h-500 | 56.2 | 70.5 | 18.2 | 3.0 | 3.0 |
| EtOH/ult-2 h-500 | 52.6 | 65.7 | 17.2 | 3.2 | 2.7 |
| EtOH/ult-24 h-500 | 51.7 | 58.6 | 15.2 | 2.7 | 1.4 |

[a] Conditions: reaction temperature 350 °C, $BaSO_4$ catalyst: 0.25 g, feed flow rate: 1.2 mL $h^{-1}$, WHSV = 5 $h^{-1}$, LA feedstock: 20 wt% in water, carrier gas $N_2$: 30 mL $min^{-1}$, TOS = 4–9 h.

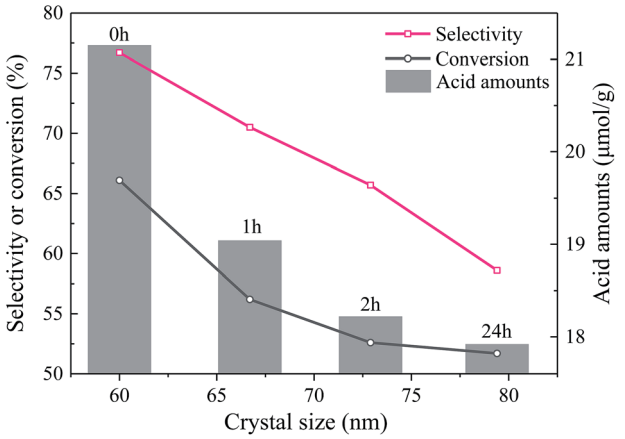


Fig. 5 Relationship between catalytic performances, crystal size and acid amounts.

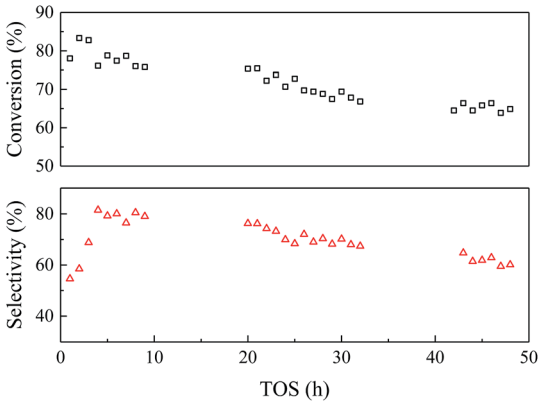


Fig. 6 Catalyst stability of EtOH/ult-0 h-500 within 48 h. Temperature 350 °C, WHSV = 2.5 $h^{-1}$, LA feedstock: 20 wt% in water, carrier gas $N_2$: 30 mL $min^{-1}$.

**3.2.3. Effect of catalyst calcination temperature.** The effects of the calcination temperature on the catalytic performance of EtOH/ult-0 h catalyst were summarized in Table 5. The sample calcined at 350 °C, which gave a higher conversion and lower selectivity because of the carbonate residues, was not taken into account for its residue of deposited ethanol. The LA conversion significantly decreased from 66.1% to 45.8% to 28.2% with increasing calcination temperature from 500 °C to 600 °C to 700 °C. Meanwhile, the AA selectivity decreased from 76.7% to 59.2% when the calcination temperature increased from 500 °C to 600 °C. The reason for this decrease in catalytic efficiency was the decrease of acid sites from 21.15 μmol $g^{-1}$ at 500 °C to 11.22 μmol $g^{-1}$ at 600 °C and 2.22 μmol $g^{-1}$ at 700 °C, which was also due to the reduction of crystal defects (Fig. S3b†) and surface area (Table 1). The AA selectivity was almost unchanged when the calcination temperature increased from 600 to 700 °C, because the sharp reduction of surface area resulted in both the reduction of dehydration and other competing side reactions. Thus, the results identify EtOH/ult-0 h-500 as the most efficient catalyst for the LA dehydration.

**3.2.4. Stability and carbon deposition.** The stability of the EtOH/ult catalyst was evaluated for 48 h and the results were shown in Fig. 6. The conversion of LA and selectivity to AA decreased by about 10% and 20%, respectively, which was much better than the HAP and alkali/alkali-earth modified zeolite catalysts. For example, over $Na_2HPO_4$/NaY the AA selectivity decreased by more than 20% in 8 h because of the deactivation, instability of framework and loss of surface modifiers;[24,30] over $HAP_{1.62}$-360 the conversion of LA decreased by about 10% in 8 h.[21] The stability of the EtOH/ult catalyst in this work was similar to the $BaSO_4$ catalyst reported by Peng *et al.*[28]

Table 5 Effect of calcination temperature on catalytic performance of EtOH/ult-0 h catalysts[a]

| Catalyst | Conversion (%) | Selectivity (%) | | | |
|---|---|---|---|---|---|
| | | AA | AD | AcOH | PA |
| EtOH/ult-0 h-350 | 72.9 | 66.4 | 17.4 | 3.1 | 1.0 |
| EtOH/ult-0 h-500 | 66.1 | 76.7 | 16.4 | 2.9 | 2.0 |
| EtOH/ult-0 h-600 | 45.8 | 59.2 | 20.5 | 3.5 | 2.3 |
| EtOH/ult-0 h-700 | 28.2 | 59.4 | 21.3 | 6.6 | 3.8 |

[a] Conditions: reaction temperature 350 °C, $BaSO_4$ catalyst: 0.25 g, feed flow rate: 1.2 mL $h^{-1}$, WHSV = 5 $h^{-1}$, LA feedstock: 20 wt% in water, carrier gas $N_2$: 30 mL $min^{-1}$, TOS = 4–9 h.

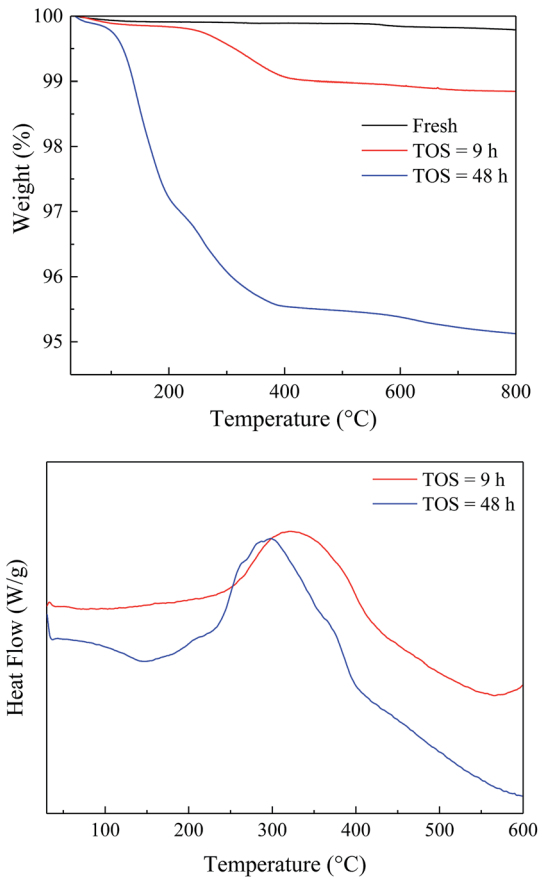


Fig. 7 TG-DTA results of the fresh and spent EtOH/ult-0 h-500 catalysts.

To study the variation of the catalysts during the reaction, the spent catalysts were analyzed by TG-DTA and the results were shown in Fig. 7. The weight loss of the spent catalyst was relatively small due to the slow carbon deposition (Table S1†). Both the EtOH/ult-0 h-500 spent for 9 and 48 h had most weight loss under 400 °C and showed a broad heat flow peak around 300 °C, indicating complex chemical composition of the deposition. Furthermore, XRD was used to study the crystal texture of the spent catalysts, and the results were shown in Fig. S6.† The intensity of diffraction peak was reduced after reaction because of the carbon deposition. No peak shift was observed in the enlarged patterns, indicating that the crystal texture was stable during the reaction and the carbon deposition should be responsible for the catalyst deactivation.

## 4. Conclusions

The structure–activity relationship of the $BaSO_4$ catalyst was studied for the dehydration reaction of LA to AA. Specific conditions such as ethanol solvent and ultrasonic treatment were employed in the co-precipitation preparation of $BaSO_4$ catalysts, and the obtained catalyst had a much smaller crystal size and more crystal defects. These catalysts, denoted as EtOH/ult, also had much higher surface area and acid amount. Further studies of the catalyst texture and binding energy revealed that the crystal defects with unbalanced electrons provided acid and basic sites, which acted as the active sites in LA dehydration. This was further confirmed by changing the catalyst preparation conditions such as the aging time and calcination temperature, in which the catalysis performance had a good correlation with the amounts of crystal defects and acid amounts. The highest surface area and acid amount were obtained over the EtOH/ult-0 h-500 catalyst, which consequently showed enhanced reaction activity (88.9% LA conversion) and selectivity (78.8% AA selectivity).

## Acknowledgements

This work was supported by the National Natural Science Foundation of China (No. 21676155).

## References

1 M. Dusselier, P. Van Wouwe, A. Dewaele, E. Makshina and B. F. Sels, *Energy Environ. Sci.*, 2013, **6**, 1415.
2 P. Gallezot, *Chem. Soc. Rev.*, 2012, **41**, 1538–1558.
3 Y. Fan, C. Zhou and X. Zhu, *Catal. Rev.*, 2009, **51**, 293–324.
4 Z. Y. Zhong, P. J. Dijkstra and J. Feijen, *J. Am. Chem. Soc.*, 2003, **125**, 11291–11298.
5 M. A. Abdel-Rahman, Y. Tashiro and K. Sonomoto, *Biotechnol. Adv.*, 2013, **31**, 877–902.
6 F. Auneau, L. S. Arani, M. Besson, L. Djakovitch, C. Michel, F. Delbecq, P. Sautet and C. Pinel, *Top. Catal.*, 2012, **55**, 474–479.
7 Y. Wang, W. Deng, B. Wang, Q. Zhang, X. Wan, Z. Tang, Y. Wang, C. Zhu, Z. Cao, G. Wang and H. Wan, *Nat. Commun.*, 2013, **4**, 2141.
8 X. Xu, J. Lin and P. Cen, *Chin. J. Chem. Eng.*, 2006, **14**, 419–427.
9 S. Varadarajan and D. J. Miller, *Biotechnol. Prog.*, 1999, **15**, 845–854.
10 Z. Zhai, X. Li, C. Tang, J. Peng, N. Jiang, W. Bai, H. Gao and Y. Liao, *Ind. Eng. Chem. Res.*, 2014, **53**, 10318–10327.
11 R. E. Holmen, Minnesota Mining and MFG, *US Pat.*, 2859240, 1958.
12 P. Sun, D. Yu, K. Fu, M. Gu, Y. Wang, H. Huang and H. Ying, *Catal. Commun.*, 2009, **10**, 1345–1349.
13 H. Wang, D. Yu, P. Sun, J. Yan, Y. Wang and H. Huang, *Catal. Commun.*, 2008, **9**, 1799–1803.
14 J. Yan, D. Yu, H. Li, P. Sun and H. Huang, *J. Rare Earths*, 2010, **28**, 803–806.
15 J. Yan, D. Yu, P. Sun and H. Huang, *Chin. J. Catal.*, 2011, **32**, 405–411.
16 D. Yu, P. Sun, Z. Tang, Z. Li and H. Huang, *Can. J. Chem. Eng.*, 2011, **89**, 484–490.
17 J. Zhang, Y. Zhao, X. Feng, M. Pan, J. Zhao, W. Ji and C. T. Au, *Catal. Sci. Technol.*, 2014, **4**, 1376.
18 G. Näfe, Y. Traa, T. Hirth and E. Klemm, *Catal. Lett.*, 2014, **144**, 1144–1150.
19 J. Zhang, X. Feng, Y. Zhao, W. Ji and C. T. Au, *J. Ind. Eng. Chem.*, 2014, **20**, 1353–1358.
20 C. Yuan, H. Liu, Z. Zhang, H. Lu, Q. Zhu and Y. Chen, *Chin. J. Catal.*, 2015, **36**, 1861–1866.
21 B. Yan, L. Z. Tao, Y. Liang and B. Q. Xu, *ACS Catal.*, 2014, **4**, 1931–1943.
22 B. Yan, L. Z. Tao, Y. Liang and B. Q. Xu, *ChemSusChem*, 2014, **7**, 1568–1578.
23 E. Blanco, C. Lorentz, P. Delichere, L. Burel, M. Vrinat, J. M. M. Millet and S. Loridant, *Appl. Catal., B*, 2016, **180**, 596–606.
24 G. Näfe, M. A. López-Martínez, M. Dyballa, M. Hunger, Y. Traa, T. Hirth and E. Klemm, *J. Catal.*, 2015, **329**, 413–424.
25 V. C. Ghantani, S. T. Lomate, M. K. Dongare and S. B. Umbarkar, *Green Chem.*, 2013, **15**, 1211.
26 E. Blanco, P. Delichere, J. M. M. Millet and S. Loridant, *Catal. Today*, 2014, **226**, 185–191.
27 Y. Matsuura, A. Onda, S. Ogo and K. Yanagisawa, *Catal. Today*, 2014, **226**, 192–197.
28 J. Peng, X. Li, C. Tang and W. Bai, *Green Chem.*, 2014, **16**, 108–111.
29 C. Tang, J. Peng, G. Fan, X. Li, X. Pu and W. Bai, *Catal. Commun.*, 2014, **43**, 231–234.
30 J. Zhang, Y. Zhao, M. Pan, X. Feng, W. Ji and C. T. Au, *ACS Catal.*, 2011, **1**, 32–41.
31 D. Wu, H. Zhu, C. Zhang and L. Chen, *Chem. Commun.*, 2010, **46**, 7250–7252.
32 H. P. Cong and S. H. Yu, *Cryst. Growth Des.*, 2009, **9**, 210–217.
33 V. Ramaswamy, R. M. Vimalathithan and V. Ponnusamy, *J. Ceram. Process. Res.*, 2011, **12**, 173–175.

34 L. Y. Chen, Y. T. Yin, C. H. Chen and J. W. Chiou, *J. Phys. Chem. C*, 2011, **115**, 20913–20919.
35 J. Wang, S. Hou, H. Chen and L. Xiang, *J. Phys. Chem. C*, 2014, **118**, 19469–19476.
36 H. Zeng, G. Duan, Y. Li, S. Yang, X. Xu and W. Cai, *Adv. Funct. Mater.*, 2010, **20**, 561–572.
37 J. Haubrich, E. Kaxiras and C. M. Friend, *Chem.–Eur. J.*, 2011, **17**, 4496–4506.
38 A. Linsebigler, G. Q. Lu and J. T. Yates, *J. Chem. Phys.*, 1995, **103**, 9438–9443.
39 T. L. Thompson and J. T. Yates, *Chem. Rev.*, 2006, **106**, 4428–4453.
40 X. Zhang, L. Lin, T. Zhang, H. Liu and X. Zhang, *Chem. Eng. J.*, 2016, **284**, 934–941.

 